Scanning Probe Microscopy Study of Layered Dichalcogenide ReS_2

S. P. Kelty,† A. F. Ruppert,† R. R. Chianelli,*,† J. Ren,‡ and M.-H. Whangbo*,‡

Contribution from the Exxon Research and Engineering Company, Annandale, New Jersey 08801, and Department of Chemistry, North Carolina State University, Raleigh, North Carolina 27695-8204

Received August 23, 1993. Revised Manuscript Received May 10, 1994•

Abstract: The surface of the layered chalcogenide ReS_2 was examined by atomic force microscopy (AFM) and scanning tunneling microscopy (STM), and the structure of ReS_2 was determined by single crystal X-ray diffraction measurements. The observed atomic-resolution AFM and STM images were analyzed by calculating the total and partial electron density distributions [$\rho(r_0)$ and $\rho(r_0,e_f)$, respectively] of a single ReS_2 layer taken from the bulk crystal structure. Our results show that the STM images are associated with the surface S atoms. The $\rho(r_0,e_f)$ plots of the two tunneling processes differ in topography from the $\rho(r_0)$ plot so that the surface atomic structure cannot be unambiguously deduced from the analysis of atomic-resolution STM images alone. Calculations of the $\rho(r_0)$ and $\rho(r_0,e_f)$ plots are essential for properly interpreting the atomic-resolution AFM and STM images.

Introduction

ReS_2 is of considerable interest as a catalytic material having potential application as a sulfur-tolerant hydrogenation and hydrodesulfurization (HDS) catalyst. The catalytic properties of ReS_2 were reviewed by Broadbent et al.[1] More recently, Farragher and Cossee suggested that the promotion of the MoS_2 by Co metal in the HDS reaction was a result of "pseudointercalation" of the MoS_2 by Co near the edge of the crystallite.[2] This creates a state which is isoelectronic and isostructural with ReS_2. It has been shown that ReS_2 is substantially more active in the HDS reaction than MoS_2,[3] and an electronic basis for this activity was established.[4] Furthermore, the relation between ReS_2 and cobalt-promoted MoS_2 was also investigated, and the "active sites" isoelectronic with those on ReS_2 were postulated to be the promoted sites.[5] The potential use of ReS_2 in environmentally important catalytic reactions such as HDS as well as the general interest in the physical and electronic properties of ReS_2 will be advanced by a thorough understanding of its electronic and structural properties. In the present work, we have undertaken scanning tunneling microscopy (STM)[6,7] and atomic force microscopy (AFM)[8,9] studies to probe the local basal plane properties of this material.

In STM, the nature of the observed images is determined by the bias voltage V_{bias} between the sample surface and the tip. The images are related to the empty states of the sample for the tip-to-surface tunneling ($V_{bias} > 0$) and to the filled states of the sample for the surface-to-tip tunneling ($V_{bias} < 0$). When the tip–surface interaction is negligible (for a large tip-to-surface distance, r_0), the tunneling current of the constant-height mode is proportional to the partial electron density $\rho(r_0,e_f)$ of the sample surface.[10] Typically, e_f is the highest occupied level for the surface-to-tip tunneling and the lowest unoccupied level for the tip-to-surface tunneling. For metals, e_f is the Fermi level. In the contact-mode AFM, a brighter feature of the AFM image is associated with a stronger repulsive force the tip feels, a greater charge overlap the tip makes with the surface, and hence a higher electron density region of the surface. Thus, atomic-resolution AFM images of layered compounds are well described by the total electron density plots, $\rho(r_0)$, of their surfaces.

A number of layered transition-metal chalcogenides have been studied by STM and AFM.[11,12] Recently, the STM images of layered compounds $ReSe_2$,[13] $NbSe_3$,[14] Nb_3X_8 (X = Cl, Br, I),[15] 1T-TaX_2 (X = S, Se),[16] and α-$RuCl_3$[17] have been analyzed on the basis of the $\rho(r_0,e_f)$ plots calculated for their layers by employing the extended Hückel tight-binding (EHTB)[18] electronic band structure method. The $\rho(r_0,e_f)$ plots are in excellent agreement with the observed STM images.[13-17] The contribution of an atom to the $\rho(r_0,e_f)$ plot is determined by the electronic and geometrical factors. Namely, it increases with increasing the atom contribution to the band levels near e_f and also with decreasing the distance between the atom and the tip. In all these chalcogenides and halides, the band levels near e_f are dominated by the transition-metal atoms because they are d-block band levels. Nevertheless, the topmost layer of any of these compounds has the surface consisting of chalcogen or halogen atoms, so that the transition-metal atoms are farther away from the tip than are the surface chalcogen or the halogen atoms.

† Exxon Research and Engineering Co.
‡ North Carolina State University.
• Abstract published in *Advance ACS Abstracts,* June 15, 1994.

(1) Broadbent, H. S.; Slaugh, L. H.; Jarvis, N. L. *J. Am. Chem. Soc.* **1954**, *76*, 1519.
(2) Farragher, A. L.; Cossee, P. *Proceedings of the 5th International Congress on Catalysis*, Palm Beach, 1972; North-Holland: Amsterdam, 1973; p 1301.
(3) Pecoraro, T. A.; Chianelli, R. R. *J. Catal.* **1981**, *67*, 430.
(4) Harris, S.; Chianelli, R. R. *J. Catal.* **1984**, *86*, 400.
(5) Harris, S.; Chianelli, R. R. *J. Catal.* **1988**, *98*, 17.
(6) Binnig, G.; Rohrer, H.; Gerber, Ch.; Weibel, E. *Phys. Rev. Lett.* **1982**, *49*, 57.
(7) Wiesendanger, R., Güntherodt, H.-J., Eds.; *Scanning Tunneling Microscopy I, II*; Springer Verlag: Heidelberg, Germany, 1992.
(8) Binnig, G.; Quate, C. F.; Gerber, Ch. *Phys. Rev. Lett.* **1985**, *55*, 394.
(9) Ruger, D.; Hansma, P. *Phys. Today* **1990**, *43* (October), 23.
(10) (a) Tersoff, J.; Hamman, D. R. *Phys. Rev. B* **1985**, *31*, 805. (b) Tersoff, J. *Phys. Rev. Lett.* **1986**, *57*, 440.
(11) Coleman, R. V.; Giambattista, B.; Hansma, P. K.; Johnson, A.; McNairy, W. W.; Slough, C. G. *Adv. Phys.* **1988**, *37*, 559.
(12) Lieber, C. M.; Wu, X. L. *Acc. Chem. Res.* **1991**, *24*, 170.
(13) Parkinson, B. A.; Ren, J.; Whangbo, M.-H. *J. Am. Chem. Soc.* **1991**, *113*, 7833.
(14) Ren, J.; Whangbo, M.-H. *Phys. Rev. B* **1992**, *46*, 4917.
(15) Magonov, S. N.; Zönnchen, P.; Rotter, H.; Cantow, H.-J.; Thiele, G.; Ren, J.; Whangbo, M.-H. *J. Am. Chem. Soc.* **1993**, *115*, 2495.
(16) Whangbo, M.-H.; Ren, J.; Canadell, E.; Louder, D.; Parkinson, B. A.; Bengel, H.; Magonov, S. N. *J. Am. Chem. Soc.* **1993**, *115*, 3760.
(17) Ren, J.; Whangbo, M.-H.; Bengel, H.; Magonov, S. N. *J. Phys. Chem.* **1993**, *97*, 4764.
(18) Whangbo, M.-H.; Hoffmann, R. *J. Am. Chem. Soc.* **1978**, *100*, 6093.

0002-7863/94/1516-7857$04.50/0

Table 1

A. Lattice Parameters and Fractional Coordinates of ReS_2

a = 6.417(4)	α = 119.06(4)
b = 6.377(4)	β = 91.62(5)
c = 6.461(4)	γ = 105.12(5)

V = 219.3(2) Å^3

d_{calcd} = 7.581 g cm^{-3}

B. Fractional Atomic Coordinates[a]

atom	x	y	z
Re(1)	0.4925(1)	0.0563(1)	0.3088(1)
Re(2)	0.4974(1)	0.4889(1)	0.2862(1)
S(1)	0.2165(10)	0.2500(10)	0.3818(9)
S(2)	0.7561(9)	0.2729(9)	0.6536(8)
S(3)	0.7230(9)	0.2287(9)	0.1112(8)
S(4)	0.3025(9)	0.2466(9)	-0.1361(8)

[a] Numbers in parentheses indicate standard deviations of the last significant digits.

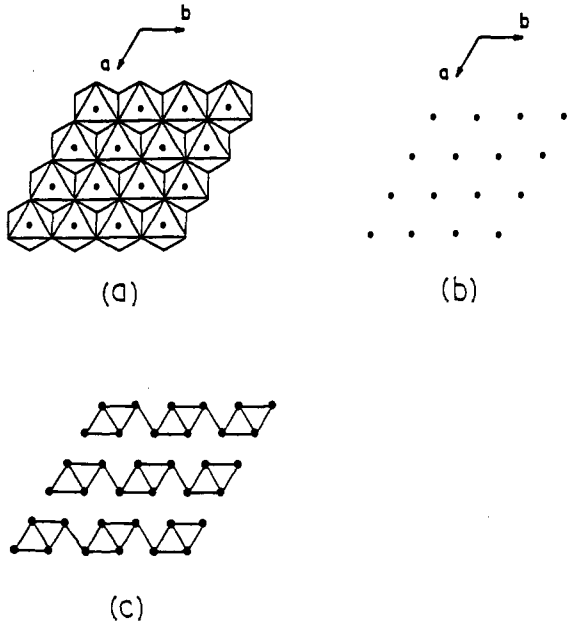

Figure 1. (a) Schematic projection view of an undistorted 1T-MX_2 layer along the c-direction (perpendicular to the layer). (b) Metal ion arrangement in an undistorted 1T-MX_2 layer. (c) Diamond-chain clustering of metal atoms in 1T-MX_2 with d^3 ions.

Consequently, the $\rho(r_0,e_f)$ plots of all these compounds are totally dominated by the surface chalcogen or halogen atoms, despite the fact that the band levels near e_f are largely made up of the metal-atom orbitals.[11-17,19]

Dichalcogenide ReS_2 is isostructural with $ReSe_2$.[20] Parkinson et al.[16] reported the STM images of $ReSe_2$ and interpreted them in terms of the $\rho(r_0,e_f)$ plots. They also reported an AFM image of $ReSe_2$ but did not provide a theoretical analysis. In a recent STM study, Freimelt et al.[21] measured STM images of ReS_2 for the surface-to-tip tunneling and suggested that the high electron density (HED) patterns of the images corresponded to the Re atoms, in contrast to the observation established for the layered chalcogenides and halides mentioned above.[13-17,19] In addition, Freimelt et al.'s work did not include STM measurements for the tip-to-surface tunneling nor AFM measurements. So far the refined atomic parameters of ReS_2 have not been reported, although ReS_2 has been known to be isostructural with $ReSe_2$.[20] In the present work, we carry out a thorough STM and AFM investigation of single crystal ReS_2, determine the structure of ReS_2 by single crystal X-ray diffraction (XRD) measurements, and analyze the observed STM and AFM images by calculating the $\rho(r_0,e_f)$ and $\rho(r_0)$ plots of a ReS_2 layer with the EHTB electronic band structure method.

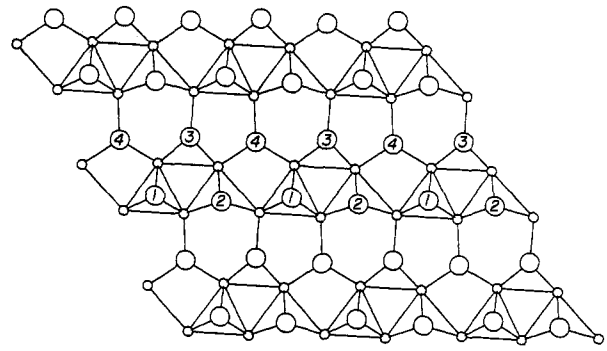

Figure 2. Schematic projection view of a ReS_2 layer along the c-direction (perpendicular to the layer). The S(1), S(2), S(3), and S(4) atoms are indicated by the numbers 1, 2, 3, and 4, respectively.

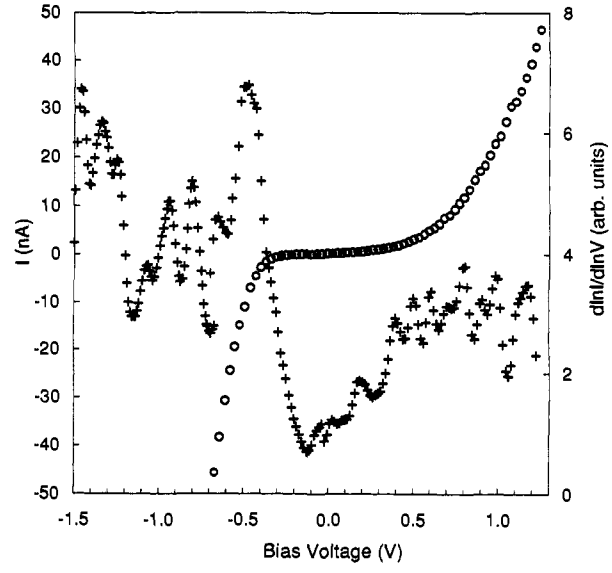

Figure 3. Tunneling current (circles) and normalized conductance (crosses) as a function of the bias voltage for ReS_2.

Structure of ReS_2

The preparation of single crystals of ReS_2 has been previously reported by Marzik et al.[22] The ReS_2 crystals used in this study were n-type ($n_d = 1 \times 10^{17}$ cm^{-3}) with an indirect optical bandgap of 1.32 eV.[22] Structural determination of this material was performed using single crystal XRD measurements.[23] A total of 1288 independent absorption-corrected reflections having 2θ (Mo Kα) < 60.4° (the equivalent of 1.3 limiting Cu Kα spheres) were collected on a computer-controlled Nicolet autodiffractometer using full (3.8° wide) ω scans and graphite-monochromated Mo Kα radiation. The structure was solved using direct methods techniques with the Siemens SHELXTL-PC software package as modified at Crystalytics Co. The resulting structural parameters have been refined to convergence [R_1 (unweighted, based on F) = 0.067 for 1098 independent absorption-corrected reflections having 2θ (Mo Kα) < 60.4° and $I > 3\sigma(I)$] using counter/weighted full-matrix least-squares techniques and a structural model which incorporated isotropic thermal parameters for all Re and S atoms. The crystals were triclinic, space group

(19) Tang, S. L.; Kasowski, R. V.; Suna, A.; Parkinson, B. A. *Surf. Sci.* **1991**, *238*, 280.

(20) (a) Alcock, N. W.; Kjekshus, A. *Acta Chem. Scand.* **1965**, *19*, 79. (b) Wildervanck, J. C.; Jellinek, F. *J. Less-Common Met.* **1971**, *24*, 73.

(21) Friemelt, K.; Akari, S.; Lux-Steiner, M. C.; Schill, T.; Bucher, E.; Dransfeld, K. *Ann. Phys. (Leipzig)* **1992**, *1*, 248.

(22) Marzik, J. V.; Kershaw, R.; Dwight, K.; Wold, A. *J. Solid State Chem.* **1984**, *51*, 170.

(23) Murray, H. H.; Kelty, S. P.; Chianelli, R. R.; Day, C. S. To be published.

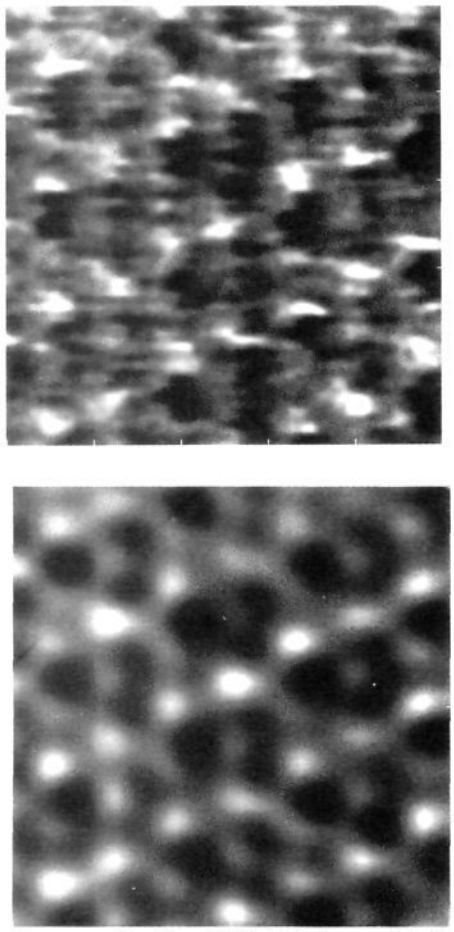

Figure 4. Representative 20- × 20-Å AFM images of ReS_2 obtained with the contact imaging mode (tip load = 4.0 nN): (top) unfiltered and (bottom) filtered.

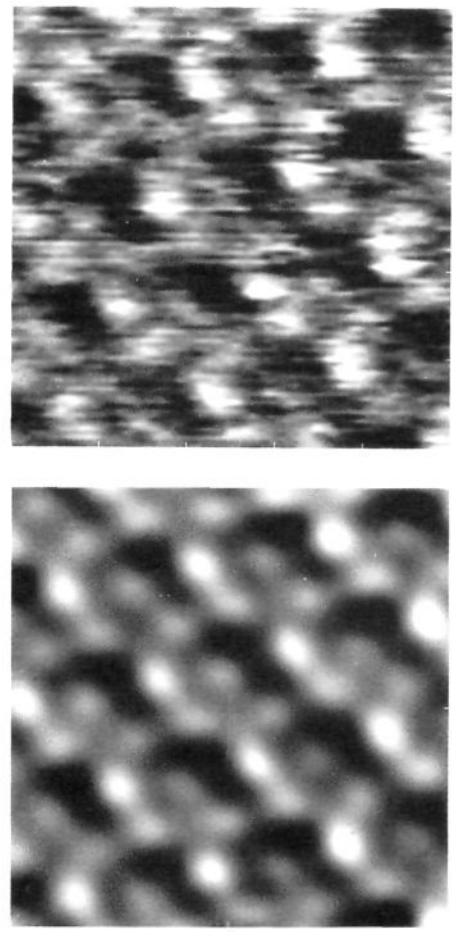

Figure 5. Representative 20- × 20-Å STM image of ReS_2 obtained with $V_{bias} = -1.40$ V and $I_{tun} = 4.5$ nA: (top) unfiltered and (bottom) filtered.

$P\bar{1}; C_i^1$ (No. 2) with unit cell parameters and the fractional atomic coordinates are summarized in Table 1.

ReX_2 (X = S, Se) can be thought of as distorted 1T-MX_2 dichalcogenides.[24] The 1T-MX_2 phases consist of edge-shared MX_6 octahedra (Figure 1a). In each MX_2 layer, the metal-atom sheet is sandwiched by chalcogen-atom sheets, and the metal atoms of an undistorted MX_2 layer form a hexagonal lattice (Figure 1b). $ReSe_2$ and ReS_2 have a d^3 electron count, and their metal-atom sheets exhibit a clustering pattern of "diamond chains" (Figure 1c).[24b] The atoms comprising the Re_4 "diamonds" are coplanar, but each diamond unit is canted by 1.43° from the basal plane (i.e., the *bc*-plane). This canting results in a 0.058-Å variation of the Re-atom heights perpendicular to the basal plane. The distortion of the Re-atom sheet from perfect hexagonal symmetry results in a distortion of the S sheets both perpendicular and parallel to the basal plane. Figure 2 shows a projection view of the surface S atoms and the subsurface Re atoms of a single ReS_2 layer. From the basal plane, the S(1) atom is most protruded, and the relative heights of the S(1), S(2), S(3), and S(4) atoms are 0.00, –0.17, –0.37, and –0.54 Å, respectively; that is, the tip–sulfur-atom distance decreases in the order S(1) > S(2) > S(3) > S(4) atoms.

(24) For reviews on the charge density wave phenomena in transition-metal dichalcogenides, see: (a) Wilson, J. A.; DiSalvo, F. J.; Mahajan, S. *Adv. Phys.* **1975**, *24*, 117. (b) Williams, P. M. In *Crystallography and Crystal Chemistry of Materials with Layered Structures*; Lévy, F., Ed.; Reidel: Dordrecht, The Netherlands, 1976; Vol. 2, p 51. (c) *Structure Phase Transitions in Layered Transition Metal Compounds*; Motizuki, K., Ed.: Reidel: Dordrecht, The Netherlands, 1986. (d) Whangbo, M.-H.; Canadell, E. *J. Am. Chem. Soc.* **1992**, *114*, 9587.

STM and AFM Measurements

A commercial scanning probe microscope (Nanoscope II) was used in our experiments at ambient conditions. Samples of single crystal ReS_2 were mounted on conducting supports and cleaved prior to STM or AFM imaging. Mechanically-sharpened Pt–Ir (80:20) tips were used for STM, and Au-coated Si_3N_4 probes were used for AFM. Atomic-scale images were recorded in the height and current imaging modes for STM and in the height and force imaging modes for AFM. Some observed images were filtered by using the fast Fourier transform procedure to emphasize the periodic features of the patterns and facilitate unit cell measurements.

Figure 3 shows the tunneling current vs bias voltage (I vs V) plot measured for ReS_2 at a fixed tip position. This plot shows a diode-like behavior, and its flat region of low current (<0.5 nA) is about 0.8-V wide. Figure 3 also shows the normalized conductance ($d \ln I/d \ln V$ vs V) plot measured for ReS_2. This plot is considered to reflect the electronic density of states (DOS) values.[25] The slope of the I vs V plot is greater for $V_{bias} < 0$ than for $V_{bias} > 0$ and so are the $d \ln I/d \ln V$ values in general. In our measurements, stable STM images were significantly more difficult to obtain for the tip-to-surface tunneling ($V_{bias} > 0$) than for the surface-to-tip tunneling ($V_{bias} < 0$). These observations may be strongly influenced by tip-induced band bending at the semiconductor surface in addition to electronic properties of the material.

Figure 4 shows a representative AFM image of ReS_2 obtained using the force imaging mode. Figure 5 shows a representative STM image of ReS_2 for the surface-to-tip tunneling. To

(25) Hamers, R. J. *Ann. Rev. Phys. Chem.* **1989**, *40*, 531.

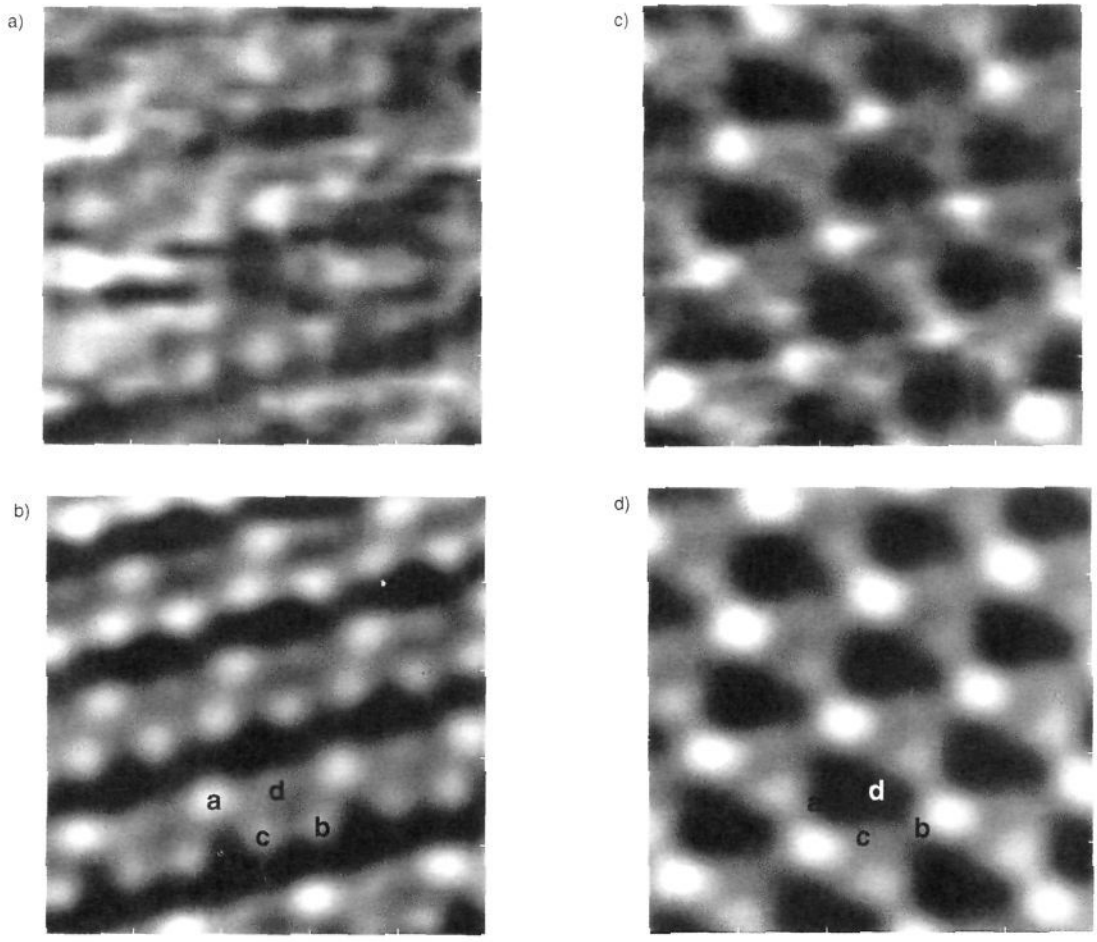

Figure 6. STM images of ReS_2 obtained with simultaneous bipolar scans. The raw and 2D Fourier transform filtered images obtained with V_{bias} = −1.60 V and I_{tun} = 12.4 nA are in parts a and b, respectively. The raw and 2D Fourier transform filtered image obtained with V_{bias} = +2.70 V and I_{tun} = 12.4 nA are in parts c and d, respectively.

emphasize the repeat patterns of these images, their filtered images obtained using the two-dimensional (2D) fast Fourier transform procedure were also presented in Figures 4 and 5. The surface unit cell parameters b, c, and α are estimated to be 6.4 ± 0.2 Å, 6.4 ± 0.2 Å, and 119 ± 0.5°, respectively, from the STM images, and 6.5 ± 0.5 Å, 6.5 ± 0.5 Å, and 120 ± 1.0°, respectively, from the AFM images. These are in good agreement with the corresponding parameters expected from the bulk crystal structure (Table 1).

The raw and 2D Fourier transform filtered STM images obtained by simultaneous bipolar scans are summarized in Figure 6a–d. Figure 6a,b shows the images for V_{bias} = −1.60 V, and Figure 6c,d, those for V_{bias} = +2.70 V. Stable STM images of this material could be obtained for $-1.8\ V < V_{bias} < -0.5$ V and $+1.5\ V < V_{bias} < +3.0$ V, although the best images were obtained within the middle portion of each voltage range. The HED patterns for $V_{bias} < 0$ (Figure 6a,b) exhibit four distinct HED spots in the repeat motif which are labeled as a, b, c, and d in Figure 6b in decreasing order of HED intensity. The labels in Figure 6d indicate the sites where the four HED spots of Figure 6b occur. Although the images for $V_{bias} > 0$ (Figure 6b,d) were recorded at the same time and location, they exhibit a significantly different HED pattern. In Figure 6d, there are only three distinct HED spots per repeat motif; there is no spot corresponding to the d site of Figure 6b. In addition, the HED sites in Figure 6b,d do not align. Many of the spots in Figure 6c,d are positioned in between those of Figure 6a,b. These differences clearly indicate different electronic origins of the HED spots in the $V_{bias} > 0$ and $V_{bias} < 0$ data.

We now consider the origin of the tunneling current in Figures 5 and 6. ReS_2 is an n-type semiconductor with an indirect optical band gap E_g = 1.32 eV,[22] and the temperature dependence of its electrical resistivity shows an activation energy E_a = 0.07 eV.[21] Thus, at room temperature, the Fermi level of ReS_2 lies within 0.07 eV below the bottom of the conduction band. The surface region bands in an n-doped semiconductor in a metal–insulator–semiconductor (MIS) junction will bend upward at zero bias (Figure 7a).[26] Under reverse bias ($V_{bias} > 0$, Figure 7b), the band bending is increased and tunneling (I_m) occurs from filled metallic tip states to empty sample states in the conduction band. Under forward bias ($V_{bias} < 0$, Figure 7c), the bands bend downward, which results in an accumulation of carriers at the bottom of the conduction band near the surface. The resulting tunneling current has components originating from the accumulated carriers both at the bottom of the conduction band (I_{cb}) and at the top of the valence band (I_{vb}). Clearly, the V_{bias} must be −1.25 V ($-[E_g - E_a]$) less for electron tunneling to occur from the top of the valence band. Given that the barrier height for electrons tunneling from the conduction band is lower than for that of the valence band electrons, one would expect images for sample-to-tip tunneling to be dominated by conduction band state density. This situation should result in tip-to-sample and sample-to-tip images being approximately the same, in contrast to our observations. To properly determine the relative contributions of the conduction and valence band state densities to the sample-to-tip tunneling images, it is necessary to consider the

(26) Sze, S. M. *Physics of Semiconductor Devices*, 2nd ed.; Wiley: New York, 1981; Chapter 5.

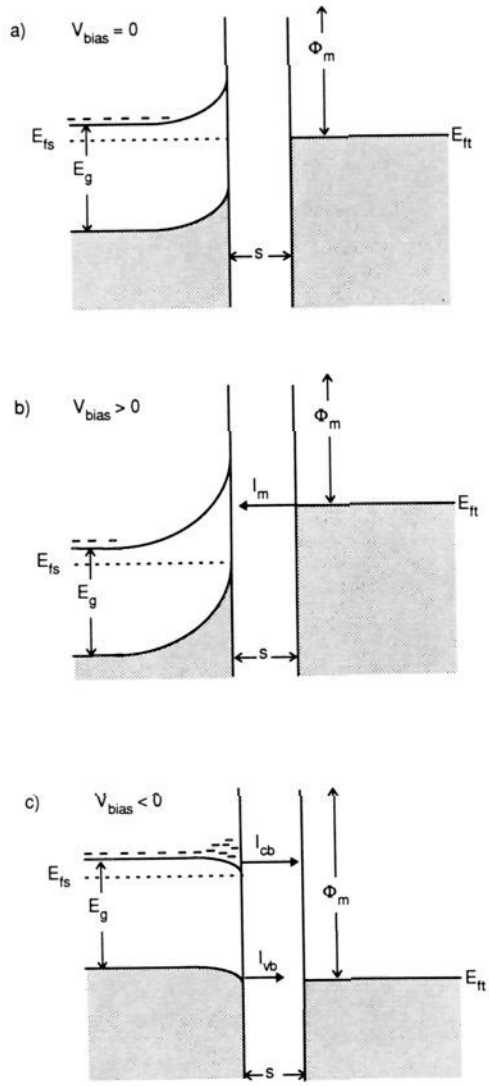

Figure 7. Energy band diagrams for an n-doped semiconductor in a MIS tunneling junction: (a) zero bias, (b) reverse bias, and (c) forward bias with accumulation.

LDOS's and occupation densities of the conduction and valence band edges. In the next section we address these issues.

Calculations of the Electronic Band Structure and Density Plots

Layered materials are characterized by covalent intralayer bonding and van der Waals interlayer interactions. Cleaving these compounds along the basal planes does not result in reconstruction so that the surface layers should be essentially identical in structure to the layers in the bulk. Therefore, we calculated the $\rho(r_0)$ and $\rho(r_0,e_f)$ plots of a single ReS_2 layer on the basis of its electronic band structure derived from the EHTB method.[18] The atomic parameters employed for our EHTB calculations were taken from the earlier work.[13,16]

Figure 8a shows the DOS plot calculated for a single ReS_2 layer in the vicinity of the valence and conduction bands. The DOS is greater at the bottom portion of the conduction band than at the top portion of the valence band. Our calculations show a band gap of 1.27 eV for a single ReS_2 layer and 0.81 eV for the three-dimensional ReS_2 lattice. The former is in approximate agreement with the optical band gap of 1.32 eV.[22] Figure 8b shows the projected DOS (PDOS) plots of the $3p_z$ orbitals of the sulfur atoms (with the z-direction perpendicular to the layer), and Figure 8c, the PDOS plots for the $3p_x$ and $3p_y$ orbitals of the sulfur atoms. It is evident from Figure 8a–c that the band levels around the band gap are dominated by the metal d orbitals. The contributions of the sulfur $3p_z$ orbitals are much stronger at the top portion of the valence band than at the bottom portion of the conduction band. For the sulfur $3p_x$ and $3p_y$ orbitals,

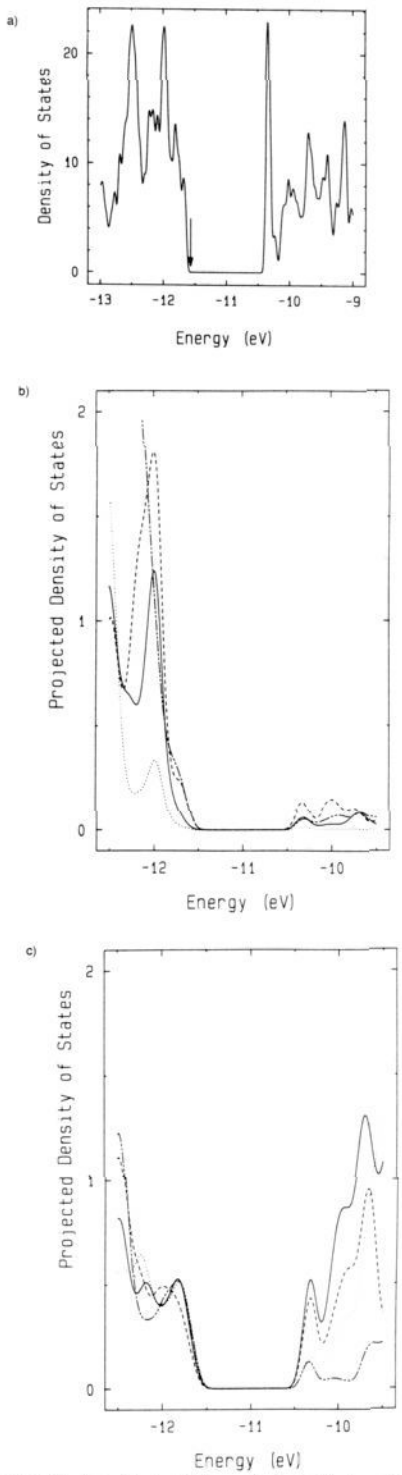

Figure 8. (a) DOS plot calculated for a single ReS_2 layer in the vicinity of the valence and conduction bands, where the arrow indicates the top of the valence band. (b) PDOS plots for the $3p_z$ orbitals of the sulfur atoms calculated for a single ReS_2 layer. The legends are as follows: solid line for S(1), dotted line for S(2), dashed line for S(3), and one-long-and-two-short dashed line for S(4). (c) PDOS plots for the $3p_x$ and $3p_y$ orbitals of the sulfur atoms calculated for a single ReS_2 layer. The legends are as follows: solid line for S(1), dotted line for S(2), dashed line for S(3), and one-long-and-two-short dashed line for S(4).

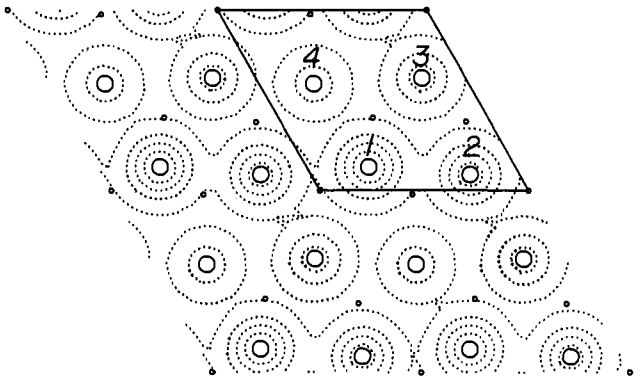

Figure 9. Two-dimensional contour representation of the $\rho(r_0)$ plot calculated for a single ReS_2 layer. The plot area consists of four unit cells, and a unit cell is indicated by the parallelogram. The contour values used are 150×10^{-3}, 100×10^{-3}, 50×10^{-3}, 10×10^{-3}, and 5×10^{-3} e/au^3. For clarity, the S atoms on the opposite surface are not shown. The Re and S atoms are shown by small and large circles, respectively. The S(1), S(2), S(3), and S(4) atoms are indicated by the numbers 1, 2, 3, and 4, respectively.

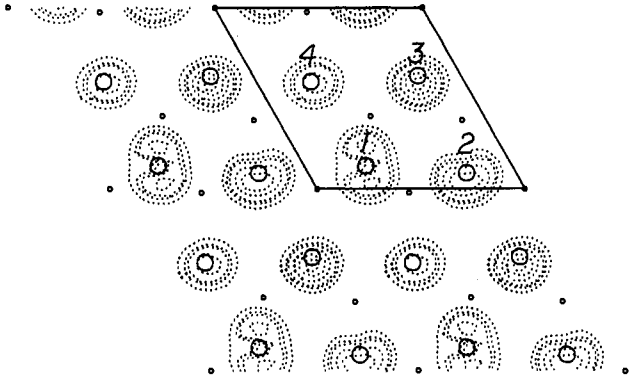

Figure 10. Two-dimensional contour representation of the $\rho(r_0,e_f)$ plot calculated for a single ReS_2 layer associated with surface-to-tip tunneling. The plot area consists of four unit cells, and a unit cell is indicated by the parallelogram. The contour values used are 25×10^{-4}, 20×10^{-4}, 15×10^{-4}, 10×10^{-4}, 8×10^{-4}, and 5×10^{-4} e/au^3. The Re and S atoms are shown by small and large circles, respectively. For clarity, the S atoms on the opposite surface are not shown. The S(1), S(2), S(3), and S(4) atoms are indicated by the numbers 1, 2, 3, and 4, respectively.

the top portion of the valence band has nearly equal contributions from all the sulfur atoms. These observations are similar to those found for $ReSe_2$.[13]

In our calculations for $\rho(r_0)$ and $\rho(r_0,e_f)$, the r_0 value was taken to be 0.5 Å (i.e., 0.5 Å away from the atoms closest to the tip). The $\rho(r_0,e_f)$ values calculated for $r_0 = 0.5$ Å have been found to accurately reflect the tunneling probabilities from a more distant tip for many layered materials.[13-17,19] Furthermore, in a simultaneous STM/AFM study of 1T-TaS_2 at ambient conditions,[27] the STM image obtained with the tip in contact with the surface is nearly identical with that of a traditional STM study.[11,12] Thus, the $\rho(r_0,e_f)$ plot calculated for a small r_0 value can be used for the interpretation of the STM images, as has been demonstrated for many layered systems.[13-17,19] We calculated the $\rho(r_0,e_f)$ plot for the surface-to-tip tunneling by employing all the band levels lying within 0.25 eV from the top of the valence band and the $\rho(r_0,e_f)$ plot for the tip-to-surface tunneling by employing all the band levels lying within 0.25 eV from the bottom of the conduction band.

Experimentally, the contrast variation of an STM current image is given by a gray scale proportional to the logarithm of the tunneling current I, i.e., $\ln(I)$. To a first approximation, the tunneling current is proportional to the partial electron density $\rho(r_0,e_f)$ so that, in principle, STM current images should be compared with $\ln[\rho(r_0,e_f)]$ plots rather than with $\rho(r_0,e_f)$ plots. The $\ln[\rho(r_0,e_f)]$ and $\rho(r_0,e_f)$ plots are different in a three-dimensional surface representation, but the topologies of the two plots are identical in a two-dimensional contour representation. In the present study, we will employ the $\rho(r_0,e_f)$ plots in a two-dimensional contour representation.

AFM Images

The $\rho(r_0)$ plot calculated for a single ReS_2 layer, shown in Figure 9, is dominated by the surface S atoms. A greater density is found on the rows of the S(1) and S(2) atoms than on those of the S(3) and S(4) atoms, as expected from the relative heights of these atoms, which decrease in the order S(1) > S(2) > S(3) > S(4). The AFM image of Figure 4 is consistent with the patterns of the $\rho(r_0)$ plot, so that the rows of the brighter spots are assigned to the rows of the S(1) and S(2) atoms. For the $\rho(r_0)$ plot, the density distribution of each atom is centered at the atomic position. These results are consistent with the refined unit cell structure of ReS_2. (Though not shown, we have also calculated the $\rho(r_0)$ plot for a single $ReSe_2$ layer. This plot is similar to that shown in Figure 9 and is in good agreement with the AFM image of $ReSe_2$ reported by Parkinson et al.[13])

(27) Barrett, R. C.; Nogami, J.; Quate, C. F. *Appl. Phys. Lett.* **1990**, *57*, 992.

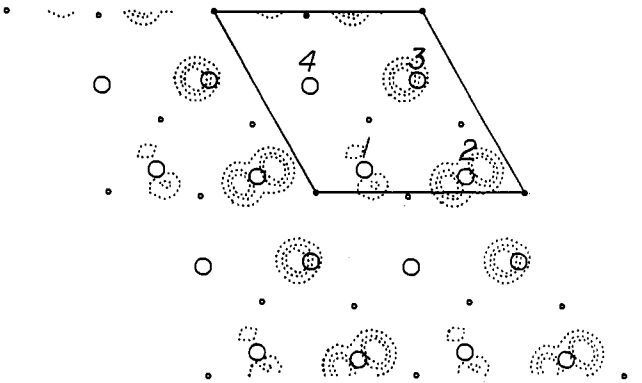

Figure 11. Two-dimensional contour representation of the $\rho(r_0,e_f)$ plot calculated for a single ReS_2 layer associated with tip-to-surface tunneling. The plot area consists of four unit cells, and a unit cell is indicated by the parallelogram. The contour values used are 10×10^{-4}, 8×10^{-4}, and 5×10^{-4} e/au^3. The Re and S atoms are shown by small and large circles, respectively. For clarity, the S atoms on the opposite surface are not shown. The S(1), S(2), S(3), and S(4) atoms are indicated by the numbers 1, 2, 3, and 4, respectively.

STM Images

Figure 10 shows the $\rho(r_0,e_f)$ plot calculated for the surface-to-tip tunneling, which is associated with the band levels at the top portion of the valence band. In this plot, the electron density on the sulfur atoms decreases in the order S(3), S(2) > S(1), S(4) despite the fact that the relative heights decrease in the order S(1) > S(2) > S(3) > S(4). Figure 11 shows the $\rho(r_0,e_f)$ plot calculated for the tip-to-surface tunneling, in which the electron density on the sulfur atoms decreases in the order S(2) > S(3) > S(1) > S(4), and the HED spots of the S(2) and S(1) atoms are not located at the atomic positions. For both the surface-to-tip and tip-to-surface tunneling processes, the $\rho(r_0,e_f)$ plots do not correspond to the metal-atom sheet but to the surface sulfur-atom sheet. As noted from Figure 8b, the contributions of the sulfur $3p_z$ orbitals are much stronger at the top portion of the valence band than at the bottom portion of the conduction band, and these orbitals, being perpendicular to the basal plane, extend out toward the tip. Consequently, the values of the $\rho(r_0,e_f)$ plot are smaller for the tip-to-surface than for the surface-to-tip tunneling by 1 order of magnitude (Figures 10 vs 11). This result establishes how the valence band might be imaged even under

accumulation conditions in the conduction band. The barrier height for electrons tunneling from the conduction band is 1.32 eV lower than that for valence band electrons, resulting in a 0.5–1-fold larger value of I_{cb} vs I_{vb} (Figure 7c) under typical conditions. However, this effect is far less important in comparison to the 10-fold larger density of states in the valence band. We therefore conclude that images in Figure 6a,b and Figure 6c,d correspond to the valence and conduction band edges, respectively.

It is noted that the $\rho(r_0,e_f)$ plot for the surface-to-tip tunneling (Figure 11) has a more isotropic HED pattern than does the $\rho(r_0,e_f)$ plot for the tip-to-surface tunneling (Figure 10). In addition, it is expected that a HED spot originating from the S(4) atom should be observed in surface-to-tip but not in tip-to-surface images. These features are clearly reflected in the STM images of the bipolar scans (Figure 6). The STM images for the surface-to-tip tunneling (Figure 6a,b) have a more isotropic intensity pattern than do the STM images for the tip-to-surface (Figure 6c,d). The least intense HED spot in the surface-to-tip (d in Figure 6b) is not observed at the corresponding location in the tip-to-surface image (Figure 6d). Thus, HED site d can be assigned as S(4). It is concluded that the STM images of ReS_2 predicted from EHTB calculations are consistent with the observed images.

Concluding Remarks

The HDS catalytic activities of ReS_2 and other transition-metal sulfides have been correlated with their electronic properties including the metal d character of the HOMO and the degree of covalency and strength of the metal–sulfur bond.[4] In the present study, the local electronic structure of ReS_2 has been calculated and experimentally mapped out. As expected from the crystal structure determinations and electronic structure calculations, four distinct atomic sites in the sulfur layer are observed. The AFM and STM images are well described by the $\rho(r_0)$ and $\rho(r_0,e_f)$ plots, respectively. For the surface-to-tip and tip-to-surface tunneling processes, the $\rho(r_0,e_f)$ plots are dominated by the surface S atoms and hence do not support the conclusion of Friemelt et al.[21] that the patterns of the STM image of ReS_2 refer to the Re atoms. The $\rho(r_0,e_f)$ plots differ in topography from the $\rho(r_0)$ plot, as has been observed for other layered compounds,[13–17] so that the structure of a surface deduced from the analysis of atomic-resolution STM images, under the assumption that bright STM spots represent the surface atomic positions, can be quite misleading. For the interpretation of atomic-resolution AFM and STM images of layered materials, calculations of their $\rho(r_0)$ and $\rho(r_0,e_f)$ plots are essential.

Acknowledgment. Work at North Carolina State University was supported by the Office of Basic Energy Sciences, Division of Materials Sciences, U.S. Department of Energy, under Grant DE-FG05-86ER45259. We are indebted to Professor A. Wold for providing the samples of single crystal ReS_2 used in this study. We also thank Dr. C. Day, Crystalytics, Inc., for XRD structure determination of the ReS_2 and Dr. H. H. Murray for helpful discussions concerning this determination.